

MODELING PRE-HARVEST STRESS-CRACKING OF RICE KERNELS PART II: IMPLEMENTATION AND USE OF THE MODEL

C. Laguë, B. M. Jenkins
ASSOC. MEMBER ASSOC. MEMBER
ASAE ASAE

ABSTRACT

The characteristics of pre-harvest stress-cracking of rice kernels are reviewed. Two finite element models developed by the authors for the prediction of the coupled diffusion of heat and moisture in the grain and for the resulting internal expansion and contraction of the kernel were implemented on a microcomputer. In both models, the rice grain is approximated as an axisymmetric body. The coupled diffusion model was validated against published experimental data. Meteorological data recorded over a 10-day period in a rice field near Davis, CA during the fall of 1987 were used in the simulation runs. Results show that the modeled kernel goes through daily cycles of global diurnal drying and nocturnal rewetting. Drying phases generate surface shrinkage of the modeled grain and compressive stresses in the endosperm while rewetting has the opposite effect. Further analysis of the diffusion characteristics of rice and of the nature of the bonds between the components of the grain is needed in order to accurately predict stress-cracking. **KEYWORDS.** Crack, Finite element, Modeling, Rice, Stress.

INTRODUCTION

Pre-harvest cracking of rice kernels has a direct effect on the head rice yield of the crop because cracked grains are more likely to break during processing (Rhind, 1962; Bhattacharya, 1980). Kernel cracking is caused by hygroscopic and, to a lesser extent, thermal strains and stresses due to internal moisture content and temperature gradients. The events that link the presence of moisture content and temperature gradients within individual rice grains and the ultimate reduction in the head rice yield of the crop occur in a chain reaction. It starts with the presence of such gradients that generate internal hygroscopic and thermal strains and stresses that, in turn, can initiate kernel cracking (Mossman, 1986).

A mathematical formulation of the pre-harvest stress-cracking problem for rice grains was developed by the authors in a companion study (Laguë and Jenkins, 1991) and was translated into two finite element models. The first model simulates the simultaneous processes of moisture transport and heat transfer within individual kernels and

between the grain and its environment. The second model predicts the internal expansion or contraction of the kernel under the action of hygroscopic and thermal stresses caused by variations of the moisture content and temperature of the grain. This paper deals with the implementation and use of these models for the prediction of pre-harvest stress-cracking of rice grains.

CHARACTERISTICS OF RICE KERNEL CRACKING

A mature rice kernel contains three major components; from the outside they are respectively: hull, bran (seed coats and germ) and endosperm (Laguë and Jenkins, 1991). The complete grain is called paddy or rough rice. Brown rice is obtained by removing the hull. Removal of the bran by abrasive milling yields the final product called white rice.

White rice absorbs moisture faster than brown rice and brown rice faster than rough rice (Kunze and Choudhury, 1972; Srinivas et al., 1978; Kunze and Prasad, 1978). Internal moisture diffusion also increases with increasing temperature or internal tensile strains (Desikachar and Subrahmanyam, 1961; Rhind, 1962; Srinivas et al., 1978; Itoh et al., 1985) but decreases with increasing internal compressive strains (Rhind, 1962). It can therefore be concluded that the hull and bran along with the presence of internal compressive strains have a retarding effect on crack formation as they contribute in reducing the liquid diffusivity of rice grain while temperature and tensile strains have the opposite effect.

Previous studies indicate that cracks start at the center of the kernel and then progress along its minor axes toward the exterior (transverse cracks), both for the absorption and desorption processes (Henderson, 1954; Matthews et al., 1970; Yamaguchi et al., 1980). Yamaguchi et al. (1981) proposed the following explanation for the formation of cracks during moisture absorption and desorption. At the beginning of desorption, the surface of the grain contracts which generates a local tensile stress that must be equilibrated by internal compressive stresses. The surface tensile stresses move further inside the grain as the moisture content of the inner regions drops and their magnitude gradually decreases. These internal tensile stresses can eventually initiate cracking. The whole process is reversed during moisture absorption. The largest tensile stresses occur in the outer layers during desorption and at the center of the kernel during moisture absorption. In both

Article was submitted for publication in May 1990; reviewed and approved for publication by the Food and Process Engineering Inst. of ASAE in February 1991.

The authors are Claude Laguë, Assistant Professor, Agricultural Engineering Dept., Laval University, Quebec City, P.Q., Canada; and Bryan M. Jenkins, Associate Professor, Agricultural Engineering Dept., University of California, Davis.

situations, internal tensile stresses are believed to be the initiators of cracking.

Surface cracks initiated by moisture desorption are irregular while moisture absorption produces straight fissures inside the grain; cracking in the latter case is usually more severe (Stermer, 1968). In a study relating kernel defects to rice breakage during milling, Indudhara Swamy and Bhattacharya (1980) noted that three different types of cracks may be found in rice kernels: single transverse cracks, multiple transverse cracks and longitudinal cracks.

IMPLEMENTATION OF THE FINITE ELEMENT MODEL

PROGRAMMING

A FORTRAN program was written to implement the two finite element models developed by Laguë and Jenkins (1991) for the prediction of pre-harvest stress-cracking. The models were then implemented on a Macintosh II microcomputer. The flowchart of the complete finite element code is presented in figure 1. The names of the principal subroutines are indicated in boldface characters. A brief description of the functions performed by each of these subroutines follows:

AVERG: computation of the mass average moisture content and temperature at the element and global levels;

PROPHM: computation of the values of the physical properties and surface transfer coefficients at the element level for the coupled diffusion problem;

ELEMHM: computation of the element conductivity matrix, $K^m_{eff}(t)$, and load vector, $F^m_{eff}(t)$, as defined in equations 33a and 33b;

ASSMBL: assembly of the element matrices and load vectors to form the global linear systems of equations 33 and 40;

SOLVE: solution of the global linear systems for the nodal unknowns;

PROPD: computation of the values of the physical properties at the element level for the internal displacements and failure problems;

ELEMD: computation of the element stiffness matrix, $K^m(t)$, and load vector, $F^m(t)$, as defined in equations 38a and 40a;

BOUNDC: introduction of the displacement boundary conditions (eq. 41a and 41b) into the global linear system for the displacement problem;

FAIL: computation of the total strain vector (eq. 42) and of the total and deviatoric stress vectors (eq. 43 and 45) at the element level; computation of the element strain energy of distortion density (eq. 44) and of its critical level for failure initiation (eq. 46).

Equation numbering in the above list refers to the study of Laguë and Jenkins (1991). The input data required by the program were divided into six sections: size of the problem (number of nodes and elements), initial node data (coordinates, temperature and moisture content), element data (connectivity, location), various control parameters defined by the user (initial and final time, number and size of the time steps, convergence criteria for successive iterations), flag for initially strained or unstrained conditions, and the field weather data at each time step.

PHYSICAL PROPERTIES AND SURFACE TRANSFER COEFFICIENTS

An exhaustive review of values and of existing regression models for the evaluation of the geometry of rice grains, of the required physical properties of rice kernels, and of the surface transfer coefficients between rice grains and the atmosphere was conducted by Laguë (1990). For medium-grain rice, the models selected for use in the finite element program are presented in Appendix A. For some properties, specific data for hull, bran and

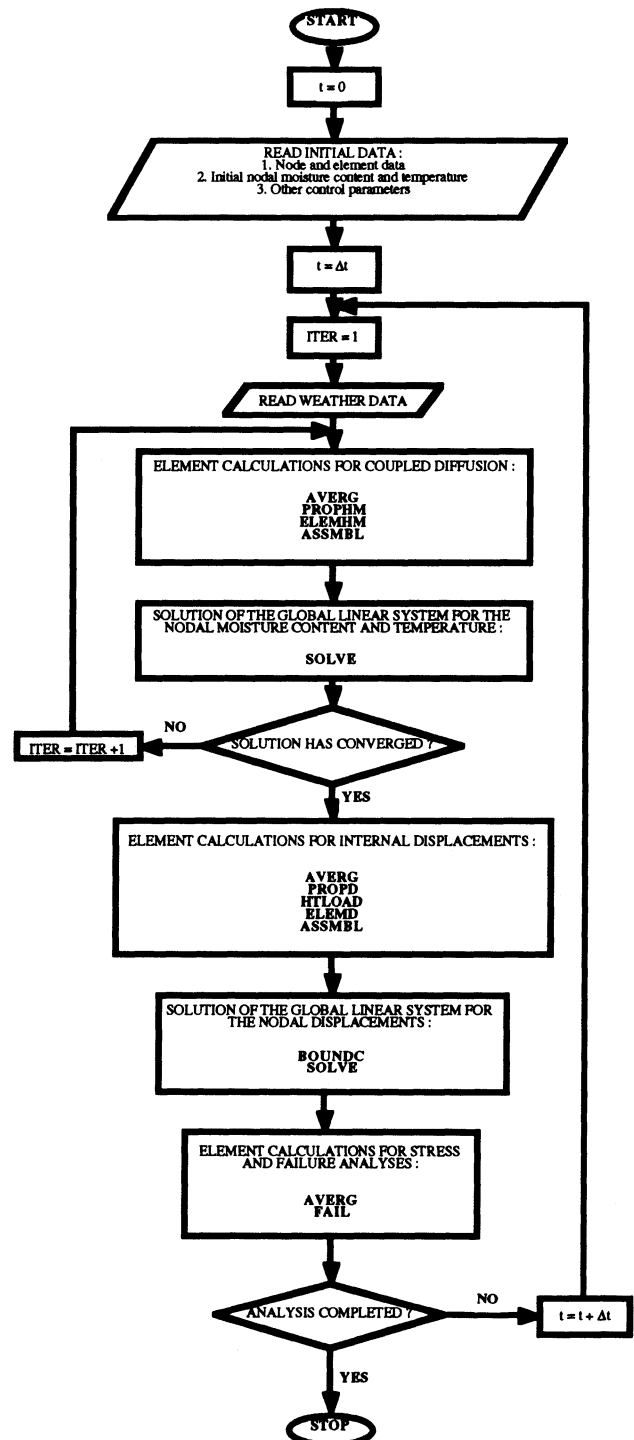


Figure 1—Finite element program flowchart.

endosperm were available whereas data for the grain as a whole existed for the other parameters.

FIELD WEATHER DATA

The meteorological data used in the simulation runs were recorded every 15 minutes in a rice field near Davis, CA between 18 September 1987 and 6 October 1987 (Jenkins, 1989) by an automatic weather station. Data for the first ten days of that period were used in the simulation runs and the same value of 15 minutes was selected for the time step. Figure 2 presents the daily fluctuations of temperature during those ten days and figure 3 illustrates the evolution of the air relative humidity during that same period of time. Finally, figure 4 shows the variations of the air velocity at the level of the rice panicle.

FINITE ELEMENT GRID

The modeled medium-grain rice kernel (fig. 5) was discretized into a 121-node/200-element grid illustrated in figure 6. Axisymmetric linear triangular elements (Laguë and Jenkins, 1991) having two degrees of freedom per node were used. As shown in figure 6, the elements are arranged in ten concentric layers around the center of the grain with the two outermost layers representing the hull, the adjacent layer accounting for the bran and the seven interior layers making up the endosperm.

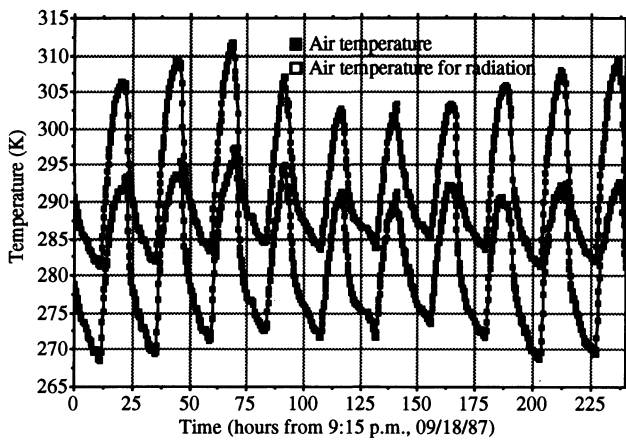


Figure 2—Temperature data for the simulation runs.

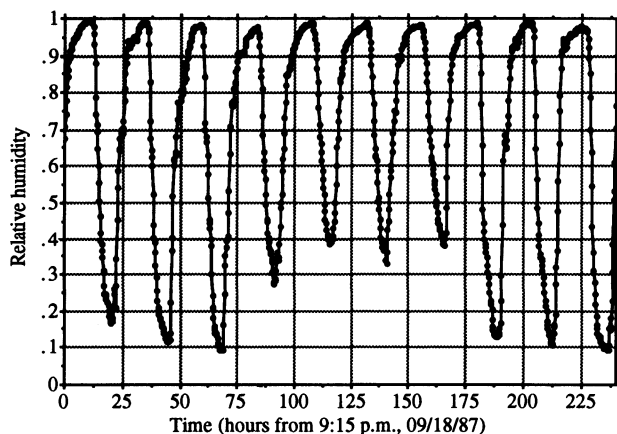


Figure 3—Air relative humidity data for the simulation runs.

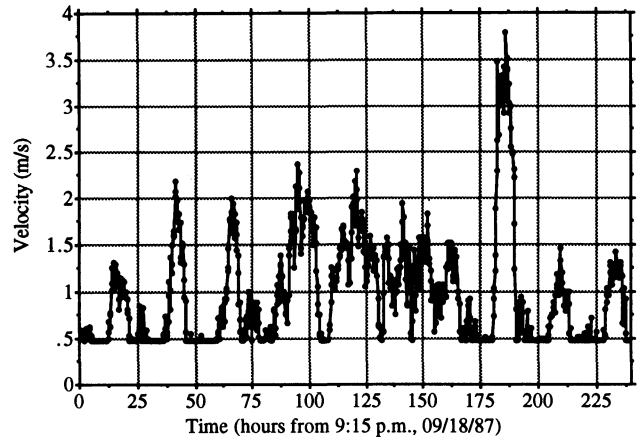


Figure 4—Air velocity data for the simulation runs.

VALIDATION OF THE FINITE ELEMENT MODELS

The finite element models developed by Laguë and Jenkins (1991) were tested against the diffusion problem in an isotropic spherical soybean kernel that was studied by Haghghi and Segerlind (1988) and also against the experimental results of Husain et al. (1973) on the drying of single rice grains. These tests allowed the coupled diffusion model to be validated. It was, however, impossible to find any useful experimental data on the internal expansion and contraction of individual grains cause by temperature and moisture gradients in order to validate the second model.

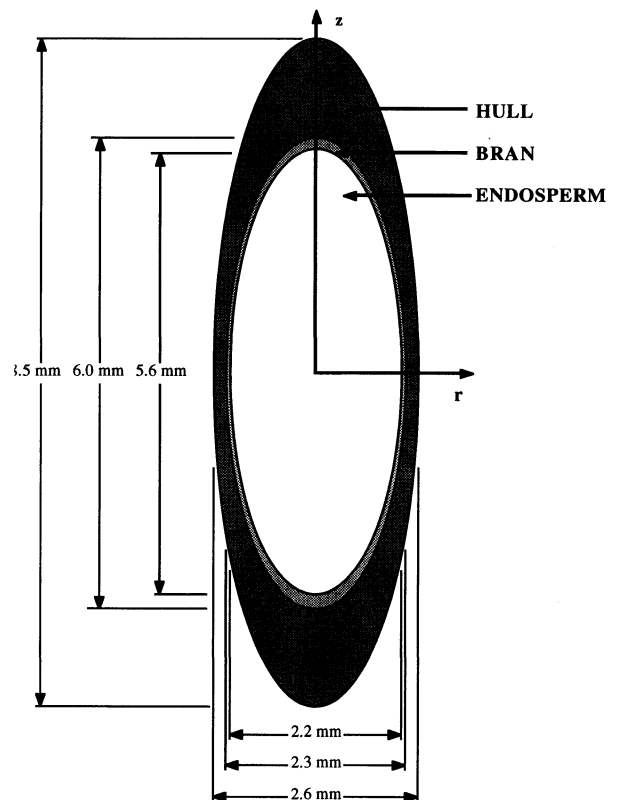


Figure 5—Initial geometry of the medium-grain rice kernel.

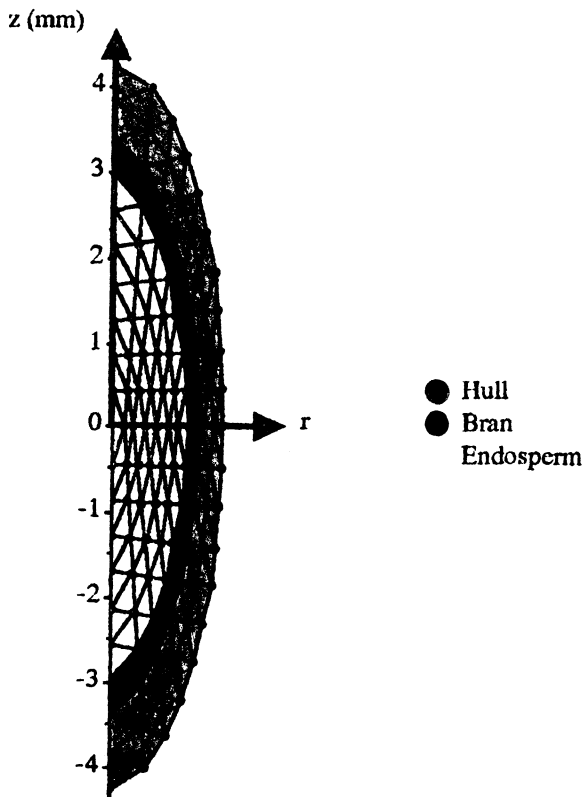


Figure 6—Finite element grid (121 nodes, 200 elements) used in the simulation runs.

In their experiments, Husain et al. (1973) used rough rice ('Bluebelle' var) having the following dimensions: length = 9.8 mm, width = 2.5 mm and thickness = 1.6 mm. To accommodate the axisymmetric model used in this study, this particular kernel was modeled as an ellipsoid with $a_i = 0.001075$ m and $b_i = 0.0049$ m (eq. A.1). The environmental conditions during their experiments were as follows: $T_{air} = 322.2$ K, $T_{airsat} = 302.5$ K, $T_{sky} = 315.5$ K, $RH_{air} = 0.22$, $V_{air} = 3.56$ m/s and $M_e = 0.07034$ kg water/kg dry grain. Husain et al. (1973) assumed the rice grain to be an isotropic material having uniform properties everywhere. The relevant physical properties of the grain were given as:

$$\frac{k}{\rho C} = 1.096 \times 10^{-8} \text{ m}^2/\text{s}$$

$$\frac{L_{wg}}{(1 + M) \rho C} = 1403 \text{ K} \cdot \text{kg dry grain/kg water}$$

$$D = \left(\frac{94.8787}{3.6 \times 10^7} \right)$$

$$\dot{e} \left(\frac{7730.65}{1.8T} \right) \left\{ e \left[\left(8.833 \times 10^{-4} \right) (1.8T) - 0.3788 \right] (100M) \right\} \text{ m}^2/\text{s}$$

The initial conditions of the kernels at the beginning of the drying experiments were uniform at: $T_0 = 295.6$ K and $M_0 = 0.26$ kg water/kg dry grain.

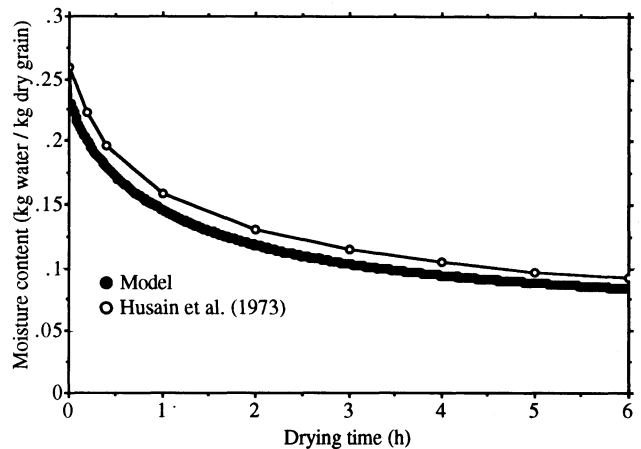


Figure 7—Predicted and experimental values of rice grain moisture content.

The finite element model for coupled diffusion was modified to accommodate the different geometry and material properties of this particular problem. However, all the surface transfer coefficients were computed according to the relations presented in Appendix A. The grid used in the validation run consisted of 121 nodes and 200 elements and a value of 1 minute was selected for the time step.

Figure 7 shows the evolution of the predicted and experimental average moisture content of the rice grain over a 6 h drying period. The predicted average moisture content is computed from the moisture content field using the mass average technique (Haghighi, 1979):

$$\bar{M}(t) = \frac{\iint_A M(r,z,t) \rho(r,z,t) r \, dr \, dz}{\iint_A \rho(r,z,t) r \, dr \, dz} \quad (1)$$

where

$\bar{M}(t)$ = mass average moisture content of the modeled grain at time t, kg water/kg dry grain;

A = cross-section of the modeled grain in the r-z plane, m².

Figure 7 shows that the average moisture content of the grain, as predicted by the model, closely follows the experimental values recorded by Husain et al. (1973). Predicted and experimental values are always within 0.01 to 0.02 kg water/kg dry grain of each other.

The comparison between predicted and experimental values of the temperature at the center of the rice grain for the first 30 minutes of drying is presented in figure 8. There is a good agreement between the predicted and observed values; the maximum difference between the two being always below 2 K. It should be noted that the model predicts a slightly faster heating of the grain center than was observed by Husain et al. (1973) at the beginning of the drying period. After about 10 minutes of drying, the trend is reversed as predicted values of kernel temperature at the center become lower than the experimental values. This may be due to the modeling of the grain geometry (ellipsoid) and of the surface heat transfer.

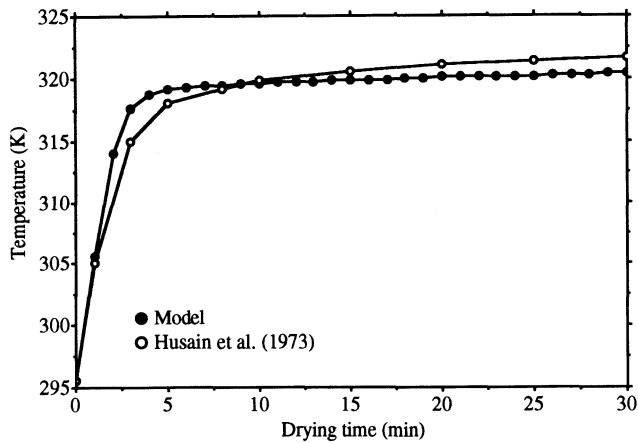


Figure 8—Predicted and observed values of temperature at the center of the rice grain.

SIMULATED CONDITIONS

Selected simulation runs were conducted using the meteorological data presented in figures 2 to 4. The modeled kernel was first assumed to be initially in a strain-free state. For that particular run, the initial conditions were selected from experimental observations (Jenkins, 1987, 1989) of kernel temperature and moisture content in the field. This translated into an initial mass average temperature of the modeled grain of 290 K and an initial mass average moisture content of 0.35 kg water/kg dry grain. Other simulations were performed to verify the effects of initial strains on the behavior of the grain. Initial strains were modeled by assuming a lower value of the initial moisture content of the grain. In these runs, the initial mass average temperature of the modeled grain was maintained at 290 K but its mass average moisture content was chosen as 0.27, 0.18, and 0.15 kg water/kg dry grain respectively.

RESULTS AND DISCUSSION

RUN # 1: STRAIN-FREE KERNEL

Figures 9 and 10 show the evolution of the predicted mass average temperature and moisture content of the modeled rice grain, as defined by equation 1, over the 10-day period covered by the simulation. The predicted kernel

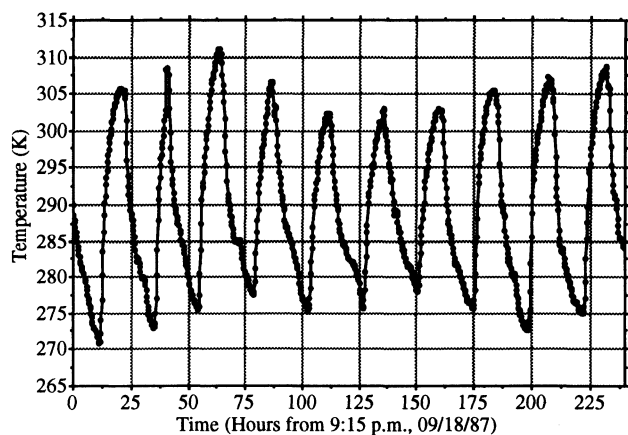


Figure 9—Predicted kernel mass average temperature.

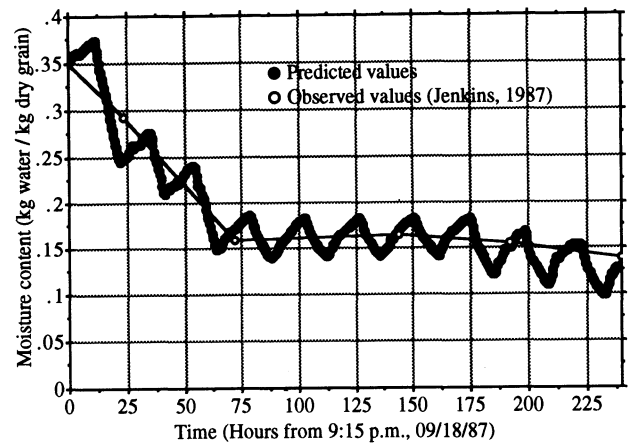


Figure 10—Predicted kernel mass average moisture content.

temperature closely matches the air temperature (fig. 2) during the day but drops below it overnight because of thermal radiation. The experimental data of Jenkins (1987) is plotted on figure 10 along with the predicted values of moisture content. One can note that the model predicts the overall drying trend of the rice grain observed during that period of time. Figure 10 also shows that the modeled kernel goes through overall drying phases during the first and last three days of the simulation because of the greater daytime drying potential (low relative humidity) of the atmosphere at that time. The model illustrates the occurrence of daily cycles of diurnal drying followed by nocturnal rewetting similar to those observed experimentally by Jenkins (1987, 1989). Figure 10 shows that the modeled grain may gain between 0.02 and 0.05 kg water/kg dry matter of moisture overnight.

Figure 11 is adapted from Jenkins (1987) and shows the evolution of the residual mass of covered and open rice windrows that were cut on the first day of his study. The 10-day simulation period of this study is indicated in the figure. Although a direct comparison of the results from figures 10 and 11 is not realistic, as figure 11 illustrates the evolution of the moisture content of the grain and straw that were forming the windrows, one can note that the

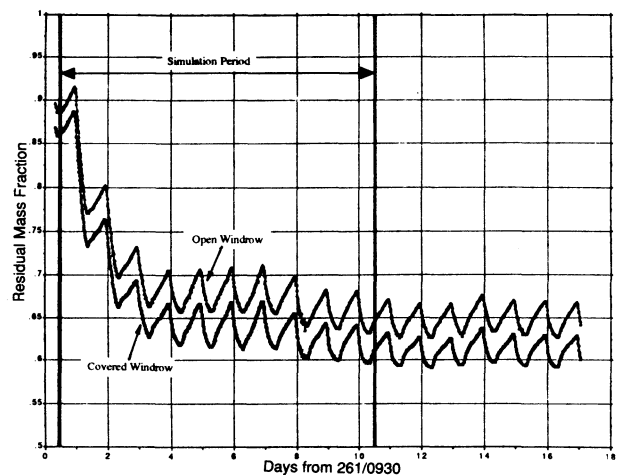


Figure 11—Total weight of rice plants in open and covered windrows (adapted from Jenkins, 1987).

general trends are similar. Both figures show cycles of nocturnal rewetting followed by diurnal drying. The experimental results of Jenkins (1987) also show that overall drying of the windrows occurred during days 0-3 and days 8-10 of the simulation period which is similar to what is predicted by the model in figure 10.

The evolution of the predicted moisture content, internal strains and stresses and of the strain energy of distortion density of the endosperm of the modeled grain was monitored. Figures 12 to 14 summarize the results obtained at the center of the kernel and at two locations on the interface bran/endosperm.

Figure 12 shows that the predicted nocturnal rewetting of the endosperm of the modeled grain is minimal. This suggests that rewetting (fig. 10) would be limited to the outer layers (hull and bran) of the grain because of the low values of liquid diffusivity used in this study and that may prevent the absorbed moisture from reaching the endosperm. This is in agreement with previous experimental observations to the effect that the hull and bran delay moisture absorption by the kernel (Kunze and Choudhury, 1972; Srinivas et al., 1978; Kunze and Prasad, 1978).

The evolution of the longitudinal strain of the endosperm of the modeled kernel is illustrated in figure 13. Daily cycles of diurnal expansion and nocturnal contraction can be observed after the second day of simulation. A similar behavior was observed for radial and tangential strains. The magnitude of the shearing strain component was very small at all times. At the end of the simulation, the endosperm of the modeled grain had shrunk by 7 to 9% in the z-direction and by 9 to 10% in the r- and θ -directions, the largest values being observed in the mid-plane region ($z = 0$). Although longitudinal shrinkage was less severe than the other two normal components, its time rate of change (slope of the strain vs. time plot) was more important.

Figure 14 illustrates the evolution of the predicted longitudinal stress at the same three locations in the modeled. Because stress is proportional to the strain rate for a viscoelastic material and since the strain rate is largest in the longitudinal direction, it is this component of stress that consistently has the largest absolute magnitude. Shearing stresses in the endosperm are very small and the

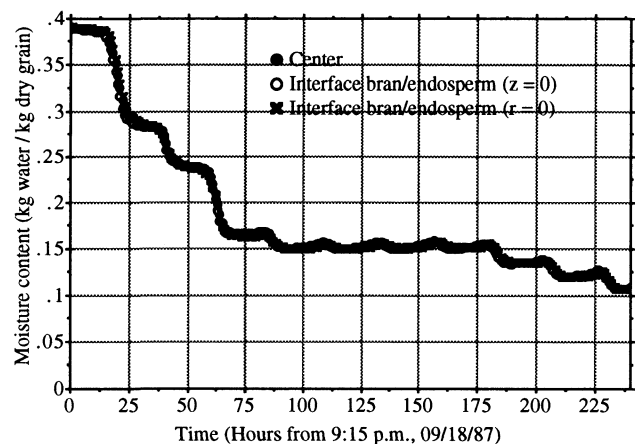


Figure 12—Evolution of the predicted moisture content at three locations in the endosperm.

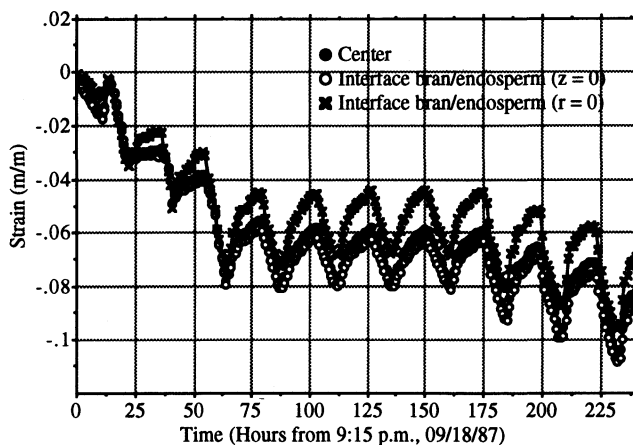


Figure 13—Evolution of the predicted longitudinal strain at three locations in the endosperm.

magnitude of the radial and tangential stresses is smaller than that of the longitudinal component. Daily cycles of stress variations within the endosperm also exist. During the day, as the mass average moisture content of the grain decreases (fig. 10), the surface of the modeled kernel (hull) contracts and experiences tensile stresses that are equilibrated by compressive stresses in the endosperm which are generated by a negative time rate of change of the longitudinal strain (fig. 13). At night, the endosperm is under tensile stresses because of a positive time rate of change of longitudinal strain (fig. 13) that equilibrates the compression of the grain surface caused by moisture absorption. A study of figures 13 and 14 reveals that peak values of both compressive and tensile stress are reached at the beginning of contraction and expansion phases of the endosperm respectively where the time rate of change of strain reaches its highest level.

The evolution of the predicted strain energy density of distortion density (SEDD) and of its critical level for failure initiation in the endosperm was also recorded during the simulation. Referring to equation 2 (where the superscript m refers to any element m within the modeled grain), it may be concluded that the critical level of SEDD will be lower when the endosperm experiences tensile stresses because: 1) the tensile strength of the modeled

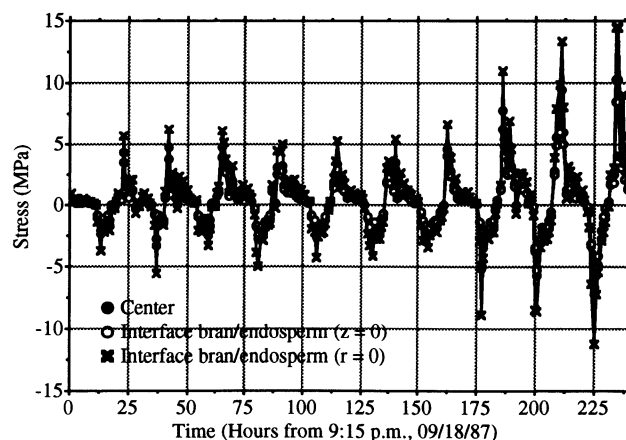


Figure 14—Evolution of the predicted longitudinal stress at three locations in the endosperm.

grain is smaller than its compressive strength (Kunze and Wratten, 1985); and 2) predicted mean tensile stresses are larger than mean compressive stresses (fig. 14).

$$\hat{\sigma}_c^m(n\Delta t) = \frac{\sigma_t^m(n\Delta t) \sigma_c^m(n\Delta t)}{6 G^m(n\Delta t)}$$

$$\pm \frac{[\sigma_t^m(n\Delta t) - \sigma_c^m(n\Delta t)] \sigma_m^m(n\Delta t)}{2 G^m(n\Delta t)} \quad (2)$$

where the “+” sign is used if element m is under a mean tensile stress and the “-” sign is used in the opposite situation.

Daily peaks in SEDD were observed when the endosperm of the modeled kernel was under maximum compressive or tensile stress, the magnitude of those peaks being greater in the latter case. This plus the fact that the critical level of SEDD is lower when the endosperm experiences tensile stresses suggest that failure is more likely to occur when the endosperm is under tensile stresses which would be in agreement with experimental observations suggesting that moisture absorption (i.e. internal tensile stresses) can initiate cracking. However, no failure was recorded in the endosperm of the modeled grain during the first run.

The behavior of the central region of the modeled kernel in the vicinity of the r-axis was studied after typical drying and rewetting phases. Figure 15 illustrates the variation of the local moisture content in that region during the first drying phase that started at t = 12 h and ended at t = 23 h and during the second rewetting phase that occurred between t = 23 h and t = 35 h. The corresponding status of the longitudinal stress in that region during the same period of time is plotted on figure 16.

Figure 15 clearly shows that the hull is losing moisture at a much higher rate than the bran and the endosperm of the modeled grain. As a result, the hull experiences large tensile stresses in the longitudinal direction at the beginning of the drying phase (fig. 16). At the same time, the inner regions of the kernel are subjected to limited compressive stresses. By the end of the drying phase, the tensile stresses have migrated inside the kernel as the inner regions also lose moisture and large compressive stresses

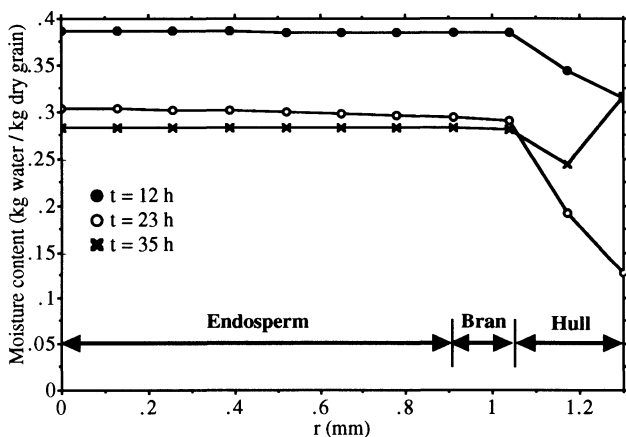


Figure 15—Predicted moisture content along the r-axis during drying and rewetting phases.

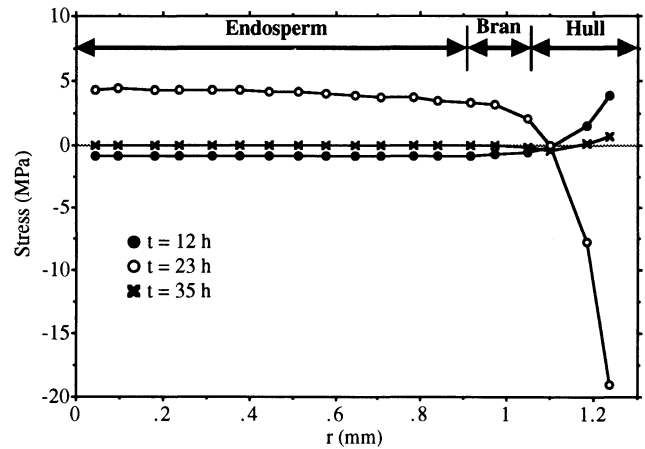


Figure 16—Predicted longitudinal stress along the r-axis during drying and rewetting phases.

in the longitudinal direction develop at the surface of the modeled kernel in order to maintain the static equilibrium of the grain. It can also be seen from figure 15 that only the outer regions of the modeled kernel (hull) gain moisture during the rewetting period while the endosperm continues to lose some moisture that diffuses to the bran and hull layers. While the surface of the grain is under large compressive stresses at the beginning of that period (t = 23 h, fig. 16 shows that the situation is reversed at the end of the rewetting period.

RUNS #2, 3 AND 4: INITIALLY STRAINED KERNEL

Three simulation runs were conducted to verify the effect of different levels of initial strains on the behavior of the modeled kernel. Detailed results for these runs may be found in Laguë (1990). The results obtained show that initial strains have little effect on kernel temperature. The initially dryer status of the kernels in these runs, however, affected the variations of the moisture content during the first few days of simulation. Higher levels of peak tensile stresses were obtained in the strained kernels but that difference gradually vanishes over the 10-day period of the simulation. This resulted in higher levels of strain energy density of distortion during the first days but these increased levels were again not sufficient to initiate failure of the endosperm.

DISCUSSION

Even if no failure of the endosperm was recorded for the first four simulation runs, the model did predict cracking for some elements located in the outer layers (hull and bran) of the modeled kernels. These cracks in the surface of the grain could in turn contribute to raise the overall liquid diffusivity of the hull and bran layers, thus contributing in more nocturnal rewetting of the endosperm. This phenomenon is very difficult to model and was not accounted for in this study. Also, superficial cracks on the grain would locally modify the stress-strain behavior of the kernel. These two phenomena would need to be studied in more detail in order to further refine the model. The model also assumed that solid bonds existed between the various components (hull, bran and endosperm) of the modeled grain and that the whole grain reacted as a solid body. Some researchers, however, suggest that a void may form

between the hull and the bran layers as the grain is drying. Additional data on that phenomenon would be needed in order to model it properly.

CONCLUSIONS

The characteristics of pre-harvest stress-cracking of rice grains were reviewed. A computer program was written to implement two finite element models developed earlier for the prediction of cracking (Laguë and Jenkins, 1991) on a microcomputer. Weather data recorded in a rice field were used as input to the model in order to predict the occurrence of stress-cracking in the field.

Results show that the coupled diffusion model correctly predicts the evolution of the kernel average moisture content in time including the daily cycles of diurnal drying and nocturnal rewetting that have been observed experimentally.

The internal expansion/contraction model also generates results consistent with previous experimental observations. Diurnal drying phases generate surface shrinkage and compressive stresses within the endosperm of the modeled grain while rewetting periods result in surface expansion and internal tensile stresses in the endosperm.

It appears that further analysis of the diffusion characteristics of the outer layers (hull and bran) of the rice kernel and of the nature of the bonds between the three major components of rough rice grains are required in order to properly predict stress-cracking of the grain.

REFERENCES

- ASAE Standards, 33rd ed. 1985. D254.4. Moisture relationships of grains. St. Joseph, MI: ASAE.
- Becker, M. 1986. *Heat Transfer: A Modern Approach*. New York: Plenum Press.
- Bhattacharya, K.R. 1980. Breakage of rice during milling: A review. *Tropical Science* 22(3):255-276.
- Chau, K.V., J.J. Gaffney and R.A. Romero. 1985. A mathematical model for the transpiration of fruits and vegetables. ASAE Paper 85-6005. St. Joseph, MI: ASAE.
- Chung, D.S. and C.H. Lee. 1986. Physical and thermal properties of grains. In *Preserving Grain Quality by Aeration and In-store Drying*, p. 53-66. Proceedings of an international seminar. Kuala Lumpur, Malaysia.
- Desikachar, H.S.R. and V. Subrahmanyam. 1961. The formation of cracks in rice during wetting and its effect on the cooking characteristics of the cereal. *Cereal Chemistry* 38(4):356-364.
- Haghighi, K. 1979. Finite element formulation of the thermo-hydro stress problem in soybeans. Unpublished Ph.D. diss. Michigan State University, East Lansing.
- Haghighi, K. and L.J. Segerlind. 1988. Modeling simultaneous heat and mass transfer in an isotropic sphere: A finite element approach. *Transactions of the ASAE* 31(2):629-637.
- Haswell, G.A. 1954. A note on the specific heat of rice, oats and their products. *Cereal Chemistry* 31(4):341-342.
- Henderson, S.M. 1954. The causes and characteristics of rice checking. *Rice Journal* 57(5):16, 18.
- Husain, A., C.S. Chen and J.T. Clayton. 1973. Simultaneous heat and mass diffusion in biological materials. *Journal of Agricultural Engineering Research* 18:343-354.
- Indudhara Swamy, Y.M. and K.R. Bhattacharya. 1980. Breakage of rice during milling: Effect of kernel defects and grain dimensions. *Journal of Food Process Engineering* 3(1):29-42.
- Itoh, K., S. Kawamura and Y. Ikeuchi. 1985. Studies on brown rice conditioning (Part 1): Experiment of thin layer conditioning. *Journal of the Society of Agricultural Machinery, Japan* 47(2):169-175.
- Jenkins, B.M. 1987. Feasibility of modified swath harvesting techniques for rice. ASAE Paper No. 87-6510. St. Joseph, MI: ASAE.
- . 1989. A modified swath harvesting technique for rice: Part I. Influence on moisture, quality, and harvester performance. *Transactions of the ASAE* 32(4):1399-1408.
- Juliano, B.O. and D.B. Bechtel. 1985. The rice grain and its gross composition, Ch. 2. In *Rice: Chemistry and Technology*, ed., B.O. Juliano. St. Paul, MN: The American Association of Cereal Chemists.
- Kunze, O.R. and M.S.U. Choudhury. 1972. Moisture adsorption related to the tensile strength of rice. *Cereal Chemistry* 49(6):684-696.
- Kunze, O.R. and S. Prasad. 1978. Grain fissuring potentials in harvesting and drying of rice. *Transactions of the ASAE* 21(2):361-366.
- Kunze, O.R. and F.T. Wratten. 1985. Physical and mechanical properties of rice, Ch. 5. In *Rice: Chemistry and Technology*, ed., B.O. Juliano. St. Paul, MN: The American Association of Cereal Chemists.
- Laguë, C. 1991. Modeling pre-harvest stress-cracking of rice kernels. Unpublished Ph.D. diss. University of California, Davis.
- Laguë, C. and B.M. Jenkins. 1991. Modeling pre-harvest stress-cracking of rice kernels: Part I: Development of a finite element model. *Transactions of the ASAE* 34(3):1797-1811.
- Massie, D.R. and K.H. Norris. 1965. Spectral reflectance and transmittance properties of grain in the visible and near infrared. *Transactions of the ASAE* 8(4):598-600.
- Matthews, J., T.J. Abadie, H.J. Deobald and C.C. Freeman. 1970. Relation between head rice yield and defective kernels in rough rice. *Rice Journal* 73(10):6-12.
- Mossman, A.P. 1986. A review of basic concepts in rice-drying research. *CRC Critical Reviews in Food Science and Nutrition* 25(1):49-71.
- Nguyen, T.V. 1985. Modeling temperature and moisture changes resulting from natural convection in grain stores. In *Preserving Grain Quality by Aeration and In-store Drying*. Proceedings of an international seminar, 81-88. Kuala Lumpur, Malaysia.
- Rhind, D. 1962. The breakage of rice in milling: A review. *Tropical Agriculture* 39:19-28.
- Sokhansanj, S. and R.J. Gustafson. 1979. Finite element prediction of rice cracking during drying. ASAE Paper No. 79-3547. St. Joseph, MI: ASAE.

- Srinivas, T., M.K. Bhashyam, M.K. Mune Gowda and H.S.R. Desikachar. 1978. Factors affecting crack formation in rice varieties during wetting and field stresses. *Indian Journal of Agricultural Science* 48(7):424-432.
- Steffe, J.F. and R.P. Singh. 1980. Liquid diffusivity of rough rice components. *Transactions of the ASAE* 23(3):767-774, 782.
- Stermer, R.A. 1968. Environmental conditions and stress cracks in milled rice. *Cereal Chemistry* 45(4):365-373.
- Webb, B.D. 1980. Rice quality and grades, Ch. 15. In *Rice: Production and Utilization*, 543-565, ed., B.S. Luh. Westport, CN: The AVI Publishing Co., Inc.
- Wratten, F.T., W.D. Poole, J.L. Chesness, S. Bal and V. Ramarao. 1969. Physical and thermal properties of rough rice. *Transactions of the ASAE* 12(6):801-803.
- Yamaguchi, S., S. Yamazawa, K. Wakabarashi and K. Horiuchi. 1980. Experimental study on the internal stress cracking of rice kernel (Part 3): On the changes of cracked rice percentage during drying, moisture adsorption and preserving processes. *Journal of the Society of Agricultural Machinery*, Japan 42(3):397-402.
- Yamaguchi, S., S. Yamazawa, K. Wakabarashi and T. Tachitani. 1981. Experimental study on the internal stress cracking of rice kernel (Part 4): A study on the mechanism of stress cracking in a rice kernel. *Journal of the Society of Agricultural Machinery*, Japan 42(4):507-512.
- Yamaguchi, S., K. Wakabarashi and S. Yamazawa. 1985. Properties of brown rice kernel for calculation of drying stresses. In *Drying '85*, p. 438-444. New York: Hemisphere Publishing Corp.

APPENDIX A: PHYSICAL PROPERTIES

The values and regression models for the relevant physical and boundary parameters of medium-grain rice kernels used in this study were compiled by Laguë (1990) from an extensive review of the pertinent literature and are presented below.

KERNEL GEOMETRY

The kernel is assumed to have an ellipsoid shape (fig. 2) i.e., its width and thickness are equal. The exterior boundary of the kernel and the inner boundaries between the three components of the rice grain are described by equations of the type:

$$\left(\frac{r}{a_i}\right)^2 + \left(\frac{z}{b_i}\right)^2 = 1 \quad (\text{A.1})$$

where

$$a_i = \begin{cases} 0.0013 \text{ m} & \text{for the exterior surface} \\ 0.00115 \text{ m} & \text{for the interface hull/bran} \\ 0.0011 \text{ m} & \text{for the interface bran/endosperm} \end{cases}$$

$$b_i = \begin{cases} 0.00425 \text{ m} & \text{for the exterior surface} \\ 0.003 \text{ m} & \text{for the interface hull/bran} \\ 0.0028 \text{ m} & \text{for the interface bran/endosperm} \end{cases}$$

Values for the parameters a_i and b_i were obtained from Webb (1980).

KERNEL DENSITY

(Wratten et al., 1969; Juliano and Bechtel, 1985):

$$(\rho_i(t))^m = d_i \frac{1465 + 705 (M(t))^m}{1 + (M(t))^m} \quad (\text{A.2})$$

where

$(\rho_i(t))^m$ = density of element m in component i at time t , kg/m^3 ;

$$d_i = \begin{cases} 0.532 & \text{for } i = \text{hull} \\ 1.493 & \text{for } i = \text{bran} \\ 1.257 & \text{for } i = \text{endosperm} \end{cases}$$

$(M(t))^m$ = average moisture content of element m at time t , $\text{kg water/kg dry grain}$.

KERNEL SPECIFIC HEAT

(Haswell, 1954; Juliano and Bechtel, 1985):

$$(C_{\text{endosperm}}(t))^m = 1180 + 3766 (M^*(t))^m \quad (\text{A.3a})$$

$$(C_{\text{bran}}(t))^m =$$

$$\frac{\frac{0.125}{1} - \frac{0.875}{1201 + 3807 (M^*(t))^m}}{(C_{\text{endosperm}}(t))^m} \quad (\text{A.3b})$$

$$(C_{\text{hull}}(t))^m =$$

$$\frac{\frac{0.2}{1} - \frac{0.1}{1109 + 4477 (M^*(t))^m} - \frac{0.7}{(C_{\text{bran}}(t))^m}}{(C_{\text{endosperm}}(t))^m} \quad (\text{A.3c})$$

where

$(C_i(t))^m$ = specific heat of element m in component i at time t , J/kg-K ;

$(M^*(t))^m$ = average moisture content of element m at time t , $\text{kg water/kg wet grain}$.

KERNEL THERMAL CONDUCTIVITY

(Kunze and Wratten, 1985; Sokhansanj and Gustafson, 1979; Chung and Lee, 1986):

$$(k(t))^m = \frac{0.0637 + 0.0958 (M(t))^m}{0.656 - 0.475 (M^*(t))^m} \quad (\text{A.4})$$

where

$(k(t))^m$ = thermal conductivity of element m at time t, W/m-K;

LATENT HEAT OF VAPORIZATION OF WATER IN THE GRAIN
(Nguyen, 1985):

$$(L_{wg}(t))^m = 1000 \left(1 + 2.566 e^{-20.176 (M(t))^m} \right) (2503 - 2.386 (T(t))^m - 273) \quad (\text{A.5})$$

where

$(L_{wg}(t))^m$ = latent heat of vaporization of water in element m at time t, J/kg water;

$(T(t))^m$ = average temperature of element in time t, K.

KERNEL LIQUID DIFFUSIVITY
(Steffe and Singh, 1980):

$$(D_i(t))^m = A_i e^{-B_i/(T(t))^m} \quad (\text{A.6})$$

where

$(D_i(t))^m$ = liquid diffusivity of element m in component i at time t, m^2/s ;

$$A_i = \begin{cases} 1.344 \times 10^{-2} & \text{for } i = \text{hull} \\ 2.214 \times 10^{-4} & \text{for } i = \text{bran} \\ 7.139 \times 10^{-7} & \text{for } i = \text{endosperm} \end{cases}$$

$$B_i = \begin{cases} 7380 & \text{for } i = \text{hull} \\ 5110 & \text{for } i = \text{bran} \\ 2830 & \text{for } i = \text{endosperm} \end{cases}$$

COEFFICIENT OF LINEAR THERMAL EXPANSION
(Kunze and Wratten, 1985; Yamaguchi et al., 1985):

$$(\beta_{th}(t))^m = 0.00000312 + 0.003657 ((M(t))^m)^2 + 0.01097 ((M(t))^m)^3 \quad (\text{A.7})$$

where

$(\beta_{th}(t))^m$ = coefficient of linear thermal expansion of element m at time t, m/m-K.

COEFFICIENT OF LINEAR HYGROSCOPIC EXPANSION
(Kunze and Wratten, 1985; Yamaguchi et al., 1985):

$$(\beta_{hyg}(t))^m = \frac{0.3533 + 0.001967 \left((T(t))^m - 273 \right)}{\left(1 + \left(1.06 + 0.0059 \left((T(t))^m - 273 \right) \right) (M(t))^m \right)^{\frac{2}{3}}} \quad (\text{A.8})$$

where

$(\beta_{hyg}(t))^m$ = coefficient of linear hygroscopic expansion of element m at time t, m-kg dry matter/m-kg water.

VISCOELASTIC PROPERTIES

The relaxation moduli of the medium-grain rice kernel are given by (Yamaguchi et al., 1985):

$$(K(t))^m = 0.667 (E_1(t))^m \left(0.3 e^{-t/(\tau_1(t))^m} + 0.7 e^{-t/(\tau_2(t))^m} \right) \quad (\text{A.9a})$$

$$(G(t))^m = 0.4 (E_1(t))^m \left(0.3 e^{-t/(\tau_1(t))^m} + 0.7 e^{-t/(\tau_2(t))^m} \right) \quad (\text{A.9b})$$

where

$(K(t))^m$ = bulk relaxation modulus of element m at time t, Pa;

$(G(t))^m$ = shear relaxation modulus of element m at time t, Pa;

$$(E_1(t))^m = \frac{1.0 \times 10^{11}}{(M(t))^m (T(t))^m}, \text{ Pa} \quad (\text{A.9c})$$

$$(\tau_1(t))^m = 1.81 \times 10^5 e^{-A}, \text{ s} \quad (\text{A.9d})$$

$$(\tau_2(t))^m = 4.32 \times 10^6 e^{-A}, \text{ s} \quad (\text{A.9e})$$

$$A = 0.02 (T(t))^m + 11 (M(t))^m \quad (\text{A.9f})$$

while the temperature and moisture shift factors are given by (Yamaguchi et al., 1985):

$$(A_T(t))^m = 351 e^{-0.02(T(t))^m} \quad (\text{A.10a})$$

$$(A_M(t))^m = 6.49e^{-11(M(t))^m} \quad (\text{A.10b})$$

where

$(A_T(t))^m$ = thermal shift factor for element m at time t;

$(A_M(t))^m$ = hygroscopic shift factor for element m at time t.

ULTIMATE TENSILE AND COMPRESSIVE STRENGTH
(Kunze and Wratten, 1985):

$$(\sigma_t(t))^m = 10,000 \left[1842 + 2696 (M(t))^m - 64.29 \left((T(t))^m - 273 \right) + 1.34 \left((T(t))^m - 273 \right)^2 \right] \quad (\text{A.11a})$$

$$(\sigma_c(t))^m = 100,000 \left[2405 - 8.278 \left((T(t))^m - 273 \right) - 159.1 (M(t))^m + 3.4 \left((M(t))^m \right)^2 \right] \quad (\text{A.11b})$$

where

$(\sigma_t(t))^m$ = ultimate tensile strength of element m at time t, Pa;

$(\sigma_c(t))^m$ = ultimate compressive strength of element m at time t, Pa;

SURFACE HEAT TRANSFER COEFFICIENT BY CONVECTION
(Chau et al., 1985; Yamaguchi et al., 1985):

$$(h_c(t))_{\delta m} = 16.09 + 65.87 (V_{air}(t))^{0.53} \quad (\text{A.12})$$

where

$(h_c(t))_{\delta m}$ = surface heat transfer coefficient by convection at the exterior boundary of element m at time t, $W/m^2 \cdot K$.

SURFACE HEAT TRANSFER COEFFICIENT BY RADIATION
(Massie and Norris, 1965):

$$(h_r(t))_{\delta m} = 2.835 \times 10^{-8}$$

$$\left((T(t))_{\delta m} + T_{sky}(t) \right) \left((T(t))_{\delta m}^2 + (T_{sky}(t))^2 \right) \quad (\text{A.13})$$

where

$(h_r(t))_{\delta m}$ = surface heat transfer coefficient by radiation at the exterior boundary of element m at time t, $W/m^2 \cdot K$;

$(T(t))_{\delta m}$ = average temperature along the exterior boundary of element m at time t, K.

SURFACE HEAT TRANSFER BY CONDENSATION AND EVAPORATION OF WATER

(Becker, 1986):

$$(h_{c/e}(t))_{\delta m} = 2.69 \left((T(t))_{\delta m} - T_{airsat}(t) \right)^2 \quad (\text{A.14})$$

where

$(h_{c/e}(t))_{\delta m}$ = surface heat transfer coefficient by condensation or evaporation of water at the exterior boundary of element m at time t, $W/m^2 \cdot K$.

KERNEL EQUILIBRIUM MOISTURE CONTENT
(ASAE, 1985):

$$M_e(t) = 0.2939 - 0.04602 \ln$$

$$\left(-(T_{air}(t) - 273) \ln RH_{air}(t) \right) \quad (\text{A.15})$$

SURFACE MOISTURE TRANSFER COEFFICIENT BY DIFFUSION

(Chau et al., 1985; Yamaguchi et al., 1985):

$$(h_d(t))_{\delta m} = 0.01959 + 0.08073 (V_{air}(t))^{0.553} \quad (\text{A.16})$$

where

$(h_d(t))_{\delta m}$ = surface moisture transfer coefficient by diffusion at the exterior boundary of element m at time t, m/s.

TABLE 1. List of symbols

Symbol	Description	Units
$C(x,t)$	kernel specific heat	J/kg wet grain
$D(x,t)$	kernel liquid diffusivity	m^2/s
$G(x,t)$	bulk modulus	Pa
$k(x,t)$	kernel thermal conductivity	W/m-K
$L_{wg}(x,t)$	latent heat of vaporization of water in the grain	J/kg water
$M(x,t)$	kernel moisture content	kg water/kg dry grain
$M_0(x)$	initial kernel moisture content	kg water/kg dry grain
$M_e(t)$	kernel equilibrium moisture content	kg water/kg dry grain
r	radial coordinate	m
$RH_{air}(t)$	air relative humidity	-
t	time	s
Δt	time step	s
$T(x,t)$	kernel temperature	K
$T_0(x)$	initial kernel temperature	K
$T_{air}(t)$	air temperature	K
$T_{sky}(t)$	effective air temperature for radiation (Bliss correlation)	K
$T_{airsat}(t)$	air temperature at saturation	K
$V_{air}(t)$	air velocity at the kernel level	m/s
x	vector of spatial coordinates	m
z	longitudinal coordinate	m
$\epsilon_{ij}(x,t)$	strain component in the direction j acting on the plane perpendicular to the i axis	m/m
$\rho(x,t)$	kernel density	kg wet grain/ m^3
$\sigma_c(x,t)$	ultimate compressive stress	Pa
$\sigma_{ij}(x,t)$	stress component in the direction j acting on the plane perpendicular to the i axis	Pa
$\sigma_m(x,t)$	approximate (FEM) mean normal stress	Pa
$\sigma_t(x,t)$	ultimate tensile stress	Pa
$\wedge_d(x,t)$	strain energy of distortion density	J/ m^3
$\wedge_{dc}(x,t)$	critical strain energy of distortion density	J/ m^3